High speed terahertz modulation from metamaterials with embedded high electron mobility transistors

David Shrekenhamer,[1] **Saroj Rout,**[2] **Andrew C. Strikwerda,**[3]
Chris Bingham,[1] **Richard D. Averitt,**[3] **Sameer Sonkusale,**[2]
and Willie J. Padilla[1,*]

[1]*Department of Physics, Boston College, 140 Commonwealth Avenue, Chestnut Hill, Massachusetts 02467, USA*
[2]*NanoLab, Electrical and Computer Engineering, Tufts University, 161 College Avenue, Medford, Massachusetts 02155, USA*
[3]*Department of Physics, Boston University, Boston, Massachusetts 02215, USA*

*[*willie.padilla@bc.edu](mailto:willie.padilla@bc.edu)*

Abstract: We present a computational and experimental study of a novel terahertz (THz) device resulting from hybridization of metamaterials with pseudomorphic high electron mobility transistors (HEMTs), fabricated in a commercial gallium arsenide (GaAs) process. Monolithic integration of transistors into each unit cell permits modulation at the metamaterial resonant frequency of 0.46 THz. Characterization is performed using a THz time-domain spectrometer (THz-TDS) and we demonstrate switching values over 30%, and THz modulation at frequencies up to 10 megahertz (MHz). Our results demonstrate the viability of incorporating metamaterials into mature semiconductor technologies and establish a new path toward achieving electrically tunable THz devices.

OCIS codes: (160.3918) Metamaterials; (350.3618) Left-handed materials; (230.4110) Modulators; (300.6495) THz spectroscopy.

References and links

1. V. G. Veselago, "The electrodynamics of substances with simultaneously negative values of ε and μ," Sov. Phys. Usp. **10**, 509–514 (1968).
2. D. R. Smith, Willie J. Padilla, D. C. Vier, S. C. Nemat-Nasser, and S. Schultz, "Composite medium with simultaneously negative permeability and permittivity," Phys. Rev. Lett. **84**, 4184–4187 (2000).
3. R. A. Shelby, D. R. Smith, and S. Schultz, "Experimental verification of a negative index of refraction," Science **292**, 77–79 (2001).
4. D. Schurig, J. J. Mock, B. J. Justice, S. A. Cummer, J. B. Pendry, A. F. Starr, and D. R. Smith, "Metamaterial electromagnetic cloak at microwave frequencies," Science **314**, 977–980 (2006).
5. J. B. Pendry, "Negative refraction makes a perfect lens," Phys. Rev. Lett. **85**, 3966–3969 (2000).
6. W. J. Padilla, M. T. Aronsson, C. Highstrete, Mark Lee, A. J. Taylor and R. D. Averitt, "Electrically resonant terahertz metamaterials: theoretical and experimental investigations," Phys. Rev. B **75**, 041102 (2007).
7. H. -T. Chen, W. J. Padilla, J. M. O. Zide, A. C. Gossard, A. J. Taylor, and R. D. Averitt "Active terahertz metamaterial devices," Nature **444**, 597–600 (2006).
8. H. -T. Chen, J. F. O'Hara, A. K. Azad, A. J. Taylor, R. D. Averitt, D. B. Shrekenhamer, and W. J. Padilla "Experimental demonstration of frequency-agile terahertz metamaterials," Nat. Photonics **2**, 295–298 (2008).
9. I. Gil, J. Garcia-Garcia, J. Bonache, F. Martin, M. Sorolla, and R. Marques, "Varactor-loaded split ring resonators for tunable notch filters at microwave frequencies," Electron. Lett. **40**, 1347–1348 (2004).
10. D. Wang, L. Ran, H. Chen, M. Mu, J. A. Kong, and B.-I. Wu, "Active left-handed material collaborated with microwave varactors," Appl. Phys. Lett. **91**, 164101 (2007).

11. T. Driscoll, S. Palit, M. M. Qazilbash, M. Brehm, F. Keilmann, Byung-Gyu Chae,Sun-Jin Yun, Hyun-Tak Kim, S. Y. Cho, N. Marie Jokerst, D. R. Smith, and D. N. Basov, "Dynamic tuning of an infrared hybrid-metamaterial resonance using vanadium dioxide," Appl. Phys. Lett. **93**, 024101 (2008).

12. H.-T. Chen, S. Palit, T. Tyler, C. M. Bingham, J. M. O. Zide, J. F. O'Hara, D. R. Smith, A. C. Gossard, R. D. Averitt, W. J. Padilla, N. M. Jokerst, and A. J. Taylor, "Hybrid metamaterials enable fast electrical modulation of freely propagating terahertz waves," Appl. Phys. Lett. **93**, 091117 (2008).

13. O. Paul, C. Imhof, B. Lägel, S. Wolff, J. Heinrich, S. Höfling, A. Forchel, R. Zengerle, R. Beigang, and M. Rahm, "Polarization-independent active metamaterial for high-frequency terahertz modulation," Opt. Express **17**, 819–827 (2009).

14. H.-T. Chen, W. J. Padilla, M. J. Cich, A. K. Azad, R. D. Averitt, and A. J. Taylor. "A metamaterial solid-state terahertz phase modulator," Nat. Photonics **3**, 148–151 (2009).

15. L. Möller, J. Federici, A. Sinyukov, C. Xie, H. C. Lim, and R. C. Giles, "Data encoding on terahertz signals for communication and sensing," Opt. Lett. **33**, 393–395 (2008).

16. W. L. Chan, H.-T. Chen, A. J. Taylor, I. Brener, M. J. Cich, and D. M. Mittleman, "A spatial light modulator for terahertz beams," Appl. Phys. Lett. **94**, 213511 (2009).

17. W. Knap, J. Lusakowski, T. Parenty, S. Bollaert, A. Cappy, V. V. Popov, and M. S. Shur, "Terahertz emission by plasma waves in 60 nm gate high electron mobility transistors," Appl. Phys. Lett. **84**, 2331–2333 (2004).

18. W. Knap, Y. Deng, S. Rumyantsev, and M. S. Shur, "Resonant detection of subterahertz and terahertz radiation by plasma waves in submicron field-effect transistors," Appl. Phys. Lett. **81**, 4637–4639 (2002).

19. T. Kleine-Ostmann, P. Dawson, K. Pierz, G. Hein, and M. Koch, "Room-temperature operation of an electrically driven terahertz modulator," Appl. Phys. Lett. **84**, 3555–3557 (2004).

20. M. Dyakonov and M. Shur, "Shallow water analogy for a ballistic field effect transistor: new mechanism of plasma wave generation by DC current," Phys. Rev. Lett. **71**, 2465–2468 (1993).

21. M. Dyakonov and M. Shur, "Detection, mixing, and frequency multiplication of terahertz radiation by two-dimensional electronic fluid," IEEE Trans. Electron Dev. **43**, 380–387 (1996).

22. V. Ryzhii, I. Khmyrova, and M. Shur, "Terahertz photomixing in quantum well structures using resonant excitation of plasma oscillations," J. Appl. Phys. **91**, 1875–1881 (2002).

23. C.-Y. Chen, T.-R. Tsai, C.-L. Pan, and R.-P. Pan, "Room temperature terahertz phase shifter based on magnetically controlled birefringence in liquid crystals," Appl. Phys. Lett. **83**, 4497–4499 (2003).

24. T.-R. Tsai, C.-Y. Chen, R.-P. Pan, C.-L. Pan, and X.-C. Zhang, "Electrically controlled room temperature terahertz phase shifter with liquid crystal," IEEE Microwave Wireless Comp. Lett. **14**, 77–79 (2003).

25. T. Kleine-Ostmann, K. Pierz, G. Hein, P. Dawson, M. Marso, and M. Koch, "Spatially resolved measurements of depletion properties of large gate two-dimensional electron gas semiconductor terahertz modulators," J. Appl. Phys. **105**, 093707 (2009).

26. D. Schurig, J. J. Mock, and D. R. Smith, "Electric-field-coupled resonators for negative permittivity metamaterials," Appl. Phys. Lett. **88**, 041109 (2006).

27. P.-C. Chao, M. S. Shur, R. C. Tiberio, K. H. G. Duh, P. M. Smith, J. M. Ballingall, P. Ho, and A. Jabra, "DC and microwave characteristics of sub-0.1- μm gate-length planar-doped pseudomorphic HEMTs," IEEE Trans. Electron Dev. **36**, 461–473 (1989).

28. Y. Cai, I. Brener, J. Lopata, J. Wynn, L. Pfeiffer, J. B. Stark, Q. Wu, X. C. Zhang, and J. F. Federici, "Coherent terahertz radiation detection: Direct comparison between free-space electro-optic sampling and antenna detection," Appl. Phys. Lett. **73**, 444–446 (1998).

29. S. J. Allen, D. C. Tsui, and F. DeRosa, "Frequency dependence of the electron conductivity in the silicon inversion layer in the metallic and localized regimes," Phys. Rev. Lett. **35**, 1359–1362 (1975).

30. E. Batke and D. Heitmann, "Rapid-Scan fourier transform spectroscopy of 2-D space charge layers in semiconductors," Infrared Phys. **24**, 189–197 (1984).

31. R. Plana, L. Escotte, O. Llopis, H. Amine, T. Parra, M. Gayral, and J. Graffeuil, "Noise in AlGaAs/InGaAs/GaAs pseudomorphic HEMTs from 10 Hz to 18 GHz," IEEE Trans. Electron Dev. **40**, 852–858 (1993).

1. Introduction

The field of metamaterials has seen significant advancement leading to the demonstration of fascinating phenomena such as negative index of refraction [1–3], invisibility cloaking [4], and perfect lensing [5]. Of special interest has been the achievements made in realizing metamaterials in the *terahertz gap* (0.1-10 THz) [6, 7], where usable naturally occurring materials are somewhat rare making this a challenging area to build traditional electronic or photonic devices.

In recent years demonstration of frequency agile and tunable metamaterials have shown great potential for applications. Various methods have been utilized to achieve amplitude and frequency modulation including photodoping [8], electronic [7, 9, 10] and temperature con-
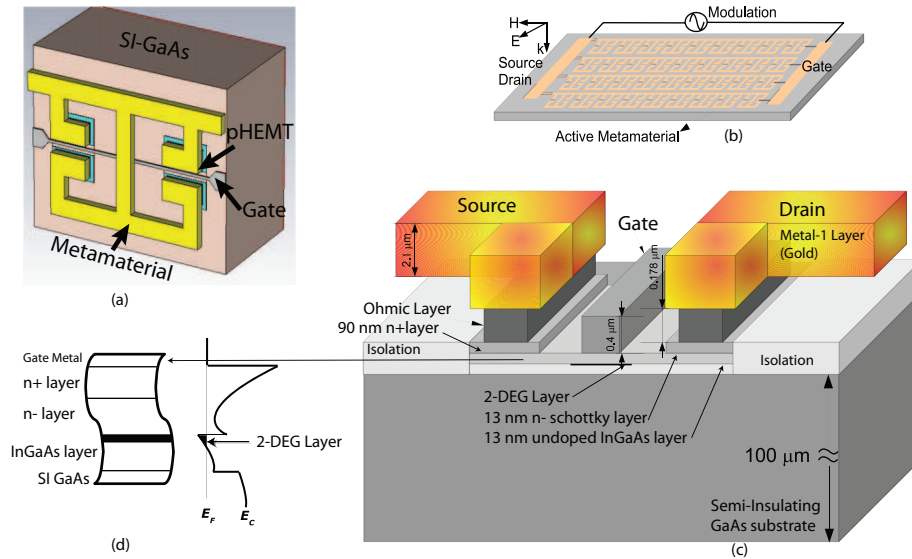
Fig. 1. Design and structure detail of the HEMT based electronically controlled THz meta-material modulator. (a) Single unit cell of the metamaterial element, as modeled for simulation. The HEMT is identified and lies under each split gap of the metamaterial. (b) Schematic depicting the entire HEMT / metamaterial device, and the polarization orientation of the incident THz wave is shown. (c) Cross-sectional view of the HEMT / metamaterial device in proximity to the split gap. (d) Band diagram detailing the 2DEG layer in the undoped InGaAs at the interface with the Schottky layer.

trol [11]. By implementing Schottky diodes other research has achieved both spatial [12, 13] and phase modulation [14]. These metamaterial devices rely on layers of n-doped gallium arsenide (GaAs) and initial studies have demonstrated the potential of these systems for high speed telecommunications [15], spectroscopy [14], and imaging [16]. To-date THz metamaterials have shown modulation at frequencies low in the MHz range, and higher speed modulation has been hindered by large device capacitance [12]. Although there has been substantial research on frequency agile and tunable metamaterials in the terahertz domain, the hybridization of semiconductor technology and metamaterials is an area of research still in its infancy.

Another area of significant research is the use of two-dimensional electron gases (2DEGs) in high electron mobility transistors and their interaction with THz waves. Studies have demonstrated the ability to create the trifecta of emission [17], detection [18], and modulation [19] of THz electromagnetic waves. The work of Dyakonov and Shur, [20, 21] has demonstrated that the 2DEG instability in short channel HEMTs has a resonant response to electromagnetic radiation at a frequency governed by the size and shape of the channel, i.e. the geometrical plasmon frequency. Tuning the plasmon resonant frequency to the incident THz wave has been used to create detectors, mixers and multipliers. Due to the non-radiative nature of 2DEG plasma oscillations (2DPs), the HEMT architecture has been implanted into a variety of structures mainly based on metal wire gratings [22]. These structures have shown broadband THz electromagnetic response at temperatures up to 300 K. When implemented as THz modulators these devices have demonstrated significant advantages over alternative architectures, such as quantum well structures which require cryogenic temperatures, and liquid crystals which possess relatively slow speeds [23, 24]. HEMT devices have thus far been limited to relatively low
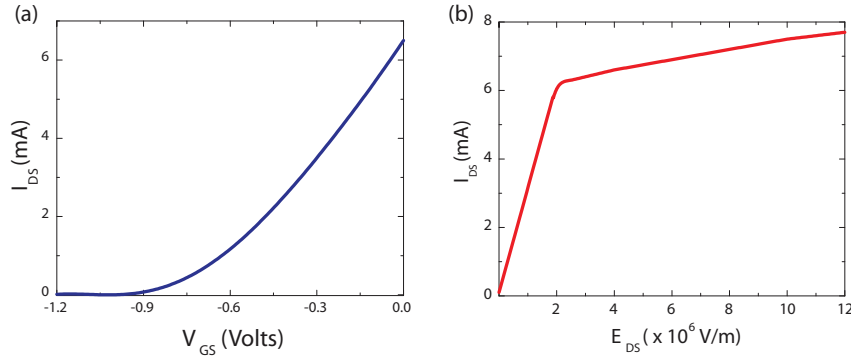
Fig. 2. The simulated I-V characteristics of the HEMT. (a) Drain-to-source current (I_{DS}) as a function of gate-to-source (V_{GS}) voltage. (b) Drain-to-source current (I_{DS}) as a function of drain-to-source electric field (E_{DS}), operating in the linear region.

transmission modulation values of less than 3%, and maximum modulation frequencies of 10 kilohertz (kHz) [25]. In this letter we demonstrate a hybrid HEMT / metamaterial device that utilizes monolithic integration of transistors *at the metamaterial unit cell level* and is able to perform as an intensity modulator at terahertz frequencies with switching speeds up to 10 MHz.

2. Design and fabrication

The sample was constructed using a commercial GaAs technology which consisted of three metal layers, an enhanced mode pseudomorphic HEMT, and a silicon nitride encapsulating dielectric, see Fig. 1. The technology utilized for this study is primarily used for mobile phone applications and to our knowledge this is the first time this has been used for THz metamaterial applications. The top metal layer, 2.1 μm thick gold, is patterned to form the metamaterial layer. A different metal layer forms the gate of the device and is also used for connecting all the gates within the same row. A 0.176 μm thick ohmic layer, which is also utilized as a routing layer, was primarily used for connecting the source and drain of the HEMT to the metamaterial. The source and drain are shorted through the metamaterial as a direct consequence of the metamaterial structure we have selected.

The metamaterial geometry used in this work is based on the electric split-ring resonator (ESRR) [6, 26], and a detail of the unit cell is shown in Fig. 1(a). Each unit cell consists of two single rings butted together with their split gaps at the outside to accommodate design rules specific to the implemented technology. The line width of the metamaterial is 4 μm and the split gap is 3 μm. The metamaterial had the dimensions of 42 μm wide by 30 μm in height. A periodic array of these unit cells as shown in Fig. 1(b) was fabricated, with period of 55 μm × 40 μm, and a total size of 2.75 × 2.6 mm^2 with 3200 elements total. Metamaterial elements are fabricated on a 100 μm thick semi-insulating (SI) GaAs substrate.

A HEMT lies underneath each of the split gaps of the metamaterial element, (two per unit cell), as shown in cross-section in Fig. 1(c). The gate length is 0.5 μm and has a width 5 μm for each device. The HEMT is constructed using pseudomorphic undoped InGaAs and a lightly doped Schottky layer, each 13 nm thick, creating a heterojunction. A 2DEG is formed in the undoped InGaAs channel layer as predicted by the band diagram at the interface (Fig. 1(d)) [27]. Unlike traditional FETs, this channel is formed in an intrinsic (undoped) crystal, resulting in very high mobility ($\sim$ 3000 cm^2/V·s) and charge density ($\sim 1.5 \times 10^{12}$ cm^{-2}) at
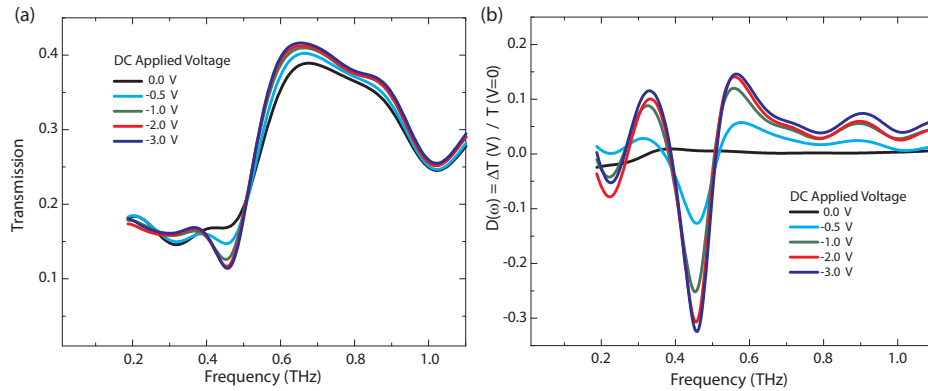
Fig. 3. (a) Frequency dependent transmitted electric field for the HEMT / metamaterial device as a function of bias. (b) Voltage dependence of the differential transmission as defined in the text.

room temperature, thus enabling fast conduction even at THz frequencies. We simulated the DC behavior of the device using Agilent's Advanced Design System (ADS) software. The dependence of the current between the source and drain terminal (I_{DS}) on the gate bias voltage (V_{GS}), and on the drain to source electric field (E_{DS}) is shown in Fig. 2(a) and 2(b), respectively.

The same metal layer which is used to form each metamaterial is also used to connect each element together within the same row. These wires run perpendicular to the split gaps, and we polarize the electric field of incident radiation perpendicular to the connecting wires which avoids the Drude-like response documented in prior works [7]. At the perimeter of the device each row is connected vertically using the ohmic layer and all elements are connected to a single bond pad to provide DC bias voltage for the drain and source of the HEMT. The gates for all HEMTs are connected in a similar fashion to a single bond pad which provides the DC bias voltage for the gate.

The entire unit cell was modeled using a commercial finite difference time domain (FDTD) solver, CST's Microwave Studio, in which the metamaterial was designed to be resonant at 0.46 THz. The physical dimensions of the material layers in the device were modeled as shown in Fig. 1(c). The gold and ohmic layers were modeled as lossy metals based on their respective DC conductivity values. For both the n+ and Schottky semiconductor layers, we utilize a frequency dependent Drude model for the conductivity. The 2DEG was simulated as a 2 nm thick Drude layer, which enables an accurate modeling of the HEMT device in both the conductive and the depleted (non-conducting) states. This is representative of what occurs in experiment by applying gate-to-source voltage (V_{GS}) of 0 V (conductive) and -1.1 V (depleted). This method allowed us to simulate the THz transmission of the device for various DC biases.

3. Results and discussion

3.1. THz transmission with DC biased HEMT

The device was characterized using a THz-TDS which has been previously described in detail [13, 28]. The incident time-domain THz electric field ($\vec{E}_i(t)$) was polarized along the split gap to drive the metamaterial elements into resonance. At the resonant frequency of the metamaterial, (0.46 THz), the electric field is concentrated within the split gaps of the metamaterial and is within the linear regime of the device owing to the low incident power used in exper-
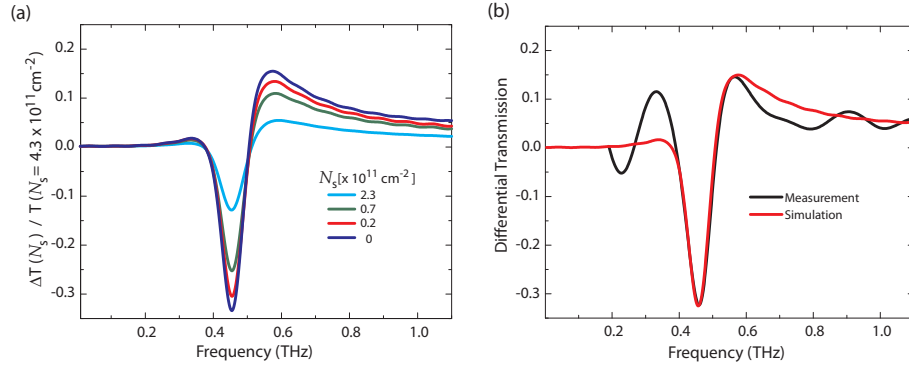
Fig. 4. (a) Simulated differential transmission for various 2D carrier concentrations N_s. (b) A comparison of simulated (red) and experimental (black) differential transmission.

iments. The reference signal was measured with the sample removed from the beam path in order to normalize the data and calculate the absolute transmission. In Fig. 3(a) we show the transmitted electric field as a function of frequency for different V_{GS} values. For V_{GS} less than -1.0 V, the channel is completely depleted, (see Fig. 2), and transmission shows a resonance at 0.46 THz. When the gate-to-source voltage is increased above -1.0 V, the channel starts forming between the split gaps, and the metamaterial resonance begins to diminish. At $V_{GS} = 0$ V, when the channel is completely formed, a low-impedance path at the split gap is created which effectively shorts the metamaterial resonant response. It can be seen in the transmission data (Fig. 3(a)) that the frequency response shows no resonance at $V_{GS} = 0$ V.

In order to elucidate the switching ability of the terahertz metamaterial, we plot the differential transmission, defined as $D(\omega) = [T(\omega)_{V_{GS}} - T(\omega)_{V_{GS}=0V}]/T(\omega)_{V_{GS}=0V}$ in Fig. 3(b). The black curve of Fig. 3(b) is two successive transmission measurements divided by each other, both at $V_{GS} = 0$ V, thus representing the frequency dependent noise. For a differential transmission of $V_{GS} = -0.5$ V, cyan curve of Fig. 3(b), $D(\omega)$ is relatively flat with deviations of about 5% or less, except at a frequency of 0.46 THz, where a value of -13% is observed. This minimum in differential transmission at 0.46 THz is seen to increase for increasing V_{GS}, until at $V_{GS} = -3.0$ V were a value of $D(\omega) = -33\%$ is observed.

We computationally investigated the combined HEMT / metamaterial system. In recent years there has been considerable interest in 2DEG formation in HEMTs as a potential candidate for far-field THz wave interaction [17–21]. A majority of these applications revolve around utilizing the 2DEG instability in the HEMT channel. In our device the plasmon resonance resulting from the 2DEG instability does not play a roll. As such the parameter of interest for us is the frequency dependent conductivity $\sigma(\omega)$. The dynamic response of the channel carriers can in many cases be described by the two-dimensional Drude conductivity [29, 30],

$$\sigma(\omega) = \frac{\sigma_0}{1 - i\omega\tau},\qquad(1)$$

which has real and imaginary parts given by:

$$\sigma_r = \sigma_0/(1 + \omega^2\tau^2), \quad \sigma_i = \sigma_0\omega\tau/(1 + \omega^2\tau^2)\qquad(2)$$

where σ_0 is the DC conductivity [Siemens / sq] given by the expression $\sigma_0 = e^2 N_s \tau/m^*$. Here e is the electron charge, N_s is the two-dimensional carrier density of the 2DEG, τ is the scattering or relaxation time, m^* is the effective mass of electrons and ω the angular frequency of
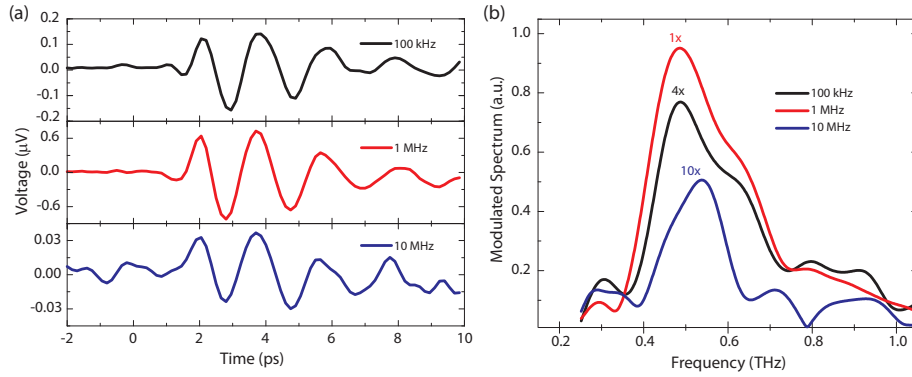
Fig. 5. (a) Time domain data for modulation at frequencies of 100 kHz, 1 MHz and 10 MHz. (b) Spectra calculated from the time domain data.

the time-varying electric field. It can be observed from Eq. (2) that for low frequencies, the conductivity is purely real and hence the current is in phase with the electric field in the split gap, for frequencies near the scattering time-constant both the real and imaginary part is half the DC conductivity and the phase is 45 degrees. For much higher frequencies the conductivity asymptotically approaches zero.

Modification of charge density in a true 2DEG has no implications on the capacitance of a metamaterial owing to its infinitesimal thickness. However, the nature of our FDTD is inherently three-dimensional. Thus, if we simply change the carrier density in simulation this would falsely modify the capacitance of the metamaterial. In order to approximate the two-dimensional charge density we restrict the real part of the permittivity to be equal to epsilon infinity (12.9 ε_0 for GaAs) and allow the imaginary part to modeled by the Drude model. The resulting complex relative permittivity can be expressed analytically as,

$$\varepsilon(\omega) = \varepsilon_\infty + i\omega_p^2 \frac{\gamma\omega^{-1}}{\omega^2 + \gamma^2}, \tag{3}$$

where γ is the collision frequency and ω_p is the plasma frequency. The collision frequency $\gamma = 2\pi \times 1.4$ THz is calculated with the relation $\gamma = e/m^*\mu$ where μ the mobility of the channel along with both e and m^* the electron charge and effective mass in GaAs. The plasma frequency is $\omega_p^2 = e^2 N_s/\varepsilon_0 m^* d$ where N_s is the two-dimensional carrier concentration and d is the simulated model thickness of the channel layer. We sweep the carrier concentration in simulation observing a full resonant metamaterial response with a completely depleted channel ($N_s = 0$ cm^{-2}) and a shorted response as the carrier concentration increased to ($N_s = 4.3$ x 10^{11} cm^{-2}), see Fig. 4(a). Comparing this simulation with the experimental data shows excellent agreement (see Fig. 4(b)).

3.2. High frequency THz modulation

In section 3.1 we demonstrated the ability to switch the THz waveform by adjusting the gate bias voltage of the HEMT with respect to the drain and source (V_{GS}). We now turn toward demonstration of high speed dynamic modulation and utilize a THz-TDS with a Photoconductive Antenna (PCA) emitter and detector. The standard mechanical chopper often utilized in a TDS system was replaced with the HEMT / metamaterial modulator which serves the same

function as the mechanical chopper with the important distinction that now only a narrow band of frequencies about the metamaterial resonance is modulated. Therefore, the data has to be interpreted differently than the static case. A square-wave bias, alternating between -1.1 V and 0 V, was applied to the gate of the HEMT with respect to the source and drain. The same square wave signal was applied to the reference input of the lock-in amplifier. After collecting the entire time-domain THz signal we have a sampled signal which can be expressed as,

$$V_{out}(t) = \alpha |\vec{E}_{t0}(t) - \vec{E}_{t1}(t)| \qquad (4)$$

where $\vec{E}_{t0}(t)$ and $\vec{E}_{t1}(t)$ are the time-domain electric-field of the transmitted THz signal when $V_{GS} = 0$ V and $V_{GS} = $ -1.1 V respectively, and α is a proportionality constant related to the particulars of the THz-TDS setup, such as the gain of pre-amplifier and averaging time-constant of the lock-in amplifier.

The time-domain signal $V_{out}(t)$ is plotted in Fig. 5(a) for three different modulation frequencies, 100 kHz, 1 MHz and 10 MHz. In Fig. 5(b) we plot the spectrum as obtained from Fourier transforming the time-domain data plotted in Fig. 5(a). It can be seen that the peak of the spectrum lies at 0.46 THz indicating modulation of the metamaterial resonance. Bandwidth of the spectrum remains relatively unchanged between 100 kHz and 1 MHz, and the amplitude of the spectrum increases. At a modulation rate of 10 MHz the bandwidth is observed to decrease a bit and the amplitude falls of from values observed at 1 MHz. The spectrum amplitude has a non-monotonic dependence as a function of frequency that can largely be attributed to the THz-TDS setup itself. PCA detection has known limitations in THz-TDS at high frequency modulation as documented in past work [28]. Contributions to the degradation of the spectrum amplitude from the HEMT / metamaterial device should remain small as there is several orders of magnitude separation between the gate-to-source modulated voltage and the input noise voltage as reported in HEMT performance studies [31]. In both the time-domain signal and the spectrum, the modulation amplitude falls off at higher frequencies and, for this device, the limit is in the neighborhood of 10 MHz. We attribute this as being primarily due to the parasitic nature of the long bond wires used in the chip assembly and, importantly, not a limitation of either the HEMT or metamaterial device.

4. Conclusion

We have demonstrated a HEMT / metamaterial device capable of modulation of THz radiation at frequencies up to 10 MHz, and modulation depths of up to 33% at 0.46 THz with all electronic control. A commercial GaAs process was utilized for implementation of the HEMT technology, as well as for fabrication of the metamaterials. We achieved monolithic integration of a total of 2×10^4 active transistors at the metamaterial unit cell level. This work demonstrates a new path for construction of high speed terahertz electronic devices.